Flow phenomena and its impact on air-sparged hydrocyclone flotation of quartz

J.D. Miller and A. Das

Abstract — *Fluid flow phenomena and therefore the flotation efficiency of air-sparged hydrocyclone (ASH) flotation are strongly dependent on operating and design variables such as air and slurry flow rates, underflow and overflow opening areas, percent solids of the feed, reagent levels, particle size and ASH length. Time-averaged multiphase flow characteristics, as determined by X-ray CT (described in a previous publication), are used to understand and explain the steady-state ASH flotation of quartz. A detailed parametric study of quartz flotation by a nominal 2-in. diam. air-sparged hydrocyclone (ASH-2C) revealed the influence of these variables on the flotation response, which is discussed in terms of the multiphase flow characteristics. Thus, a phenomenological description of quartz flotation has been established to assist in the further development and utilization of the ASH technology.*

Introduction

The high specific capacity air-sparged hydrocyclone (ASH) has been found to provide effective flotation separations in a number of applications (e.g., coal, phosphate, gold, potash, copper, wastewater treatment and deinking flotation for wastepaper recycle). The general principles of ASH flotation have been discussed in the literature (Miller, et al., 1984a, Miller, et al., 1988, Gopalakrishnan, et al., 1991, Ye, et al., 1988 and Miller, et al., 1989). Flotation in the air-sparged hydrocyclone is characterized by complex multiphase fluid-flow phenomena, which greatly influence the separation efficiency. The swirl-flow associated with ASH flotation is rotational and turbulent and involves all three phases: solid, liquid and gas. It is evident that the flow characteristics constitute a major aspect of the ASH flotation technology, and in this regard it is very important to understand how multiphase flow phenomena impact ASH flotation in order to provide a basis for improved design and operation. However, understanding the flow behavior has been limited due to experimental difficulties associated with the presence of the opaque, inner porous tube of the ASH. Conventional measurement techniques such as high-speed photography and laser-Doppler anemometry are difficult to use during actual ASH flotation experiments.

A few studies have been carried out by various researchers to understand the fundamentals of the swirl flow involved in ASH fluid dynamics. Some of the fluid dynamic aspects of swirl flow in general have been explained in terms of vorticity and swirl decay (Loader, 1981). Early ASH research to characterize the swirl flow was accomplished using a transparent plexiglass tube having no froth pedestal. In these tests, water was fed through an involute entrance at the top of the tube (Miller et al., 1984b). It was found that a wave pattern forms at the surface of the swirl layer with streamlines approximately 45 degrees from the normal when the vortex formation is complete. This led to the expectation that, under such conditions, the axial and tangential velocities are almost equal in magnitude. Also in this study (Miller, et al., 1984b), tangential and axial velocities of the swirl layer were measured using laser-Doppler anemometry. It was found that both velocities drop rapidly in the region immediately below the inlet section and then rise again. From this point downwards, the tangential velocity decays significantly with axial distance, whereas the axial velocity decays only slightly. From first principles, the radial component of velocity has to be zero at the wall and at the air/water interface. Therefore, in view of the small thickness of the swirl layer (10% of the tube radius), the radial component of velocity was assumed to be zero at all axial and radial positions in this study. Efforts were made to compare these experimentally measured tangential velocity profiles with theoretical calculations (Das, et al., 1993). In this study (Das, et al., 1993), the vorticity stream function form of the Navier-Stokes equation was solved, assuming the flow to be of high Reynolds number but still in the laminar regime. No turbulent closure equations were used.

Efforts have also been made to understand multiphase flow in the ASH by studying bubble characteristics generated from a single orifice. Consideration of the size and slip velocity of air bubbles from a single orifice (Miller, et al., 1984b) had led to speculations about multiphase flow in the ASH system. A simple theoretical expression for the size of a bubble generated at a single capillary was derived. Using a high-speed motion analyzer video system for analysis, it was found that the effect of surface tension on bubble size is negligible. Bubble coalescence does not occur at the point of formation. Bubble size increases with air rate and fluid viscosity. It was confirmed that the movement of individual bubbles follows Stoke's law. Bubble residence time was also calculated, and it was found that residence times are typically 0.2 to 0.3 sec for the aqueous phase and a few seconds for individual microbubbles. For a bubble swarm, the residence times are longer, depending on the volume fraction of the

J.D. Miller and **A. Das**, members SME, are professor and former graduate student, respectively, with the Department of Metallurgical Engineering, the University of Utah, Salt Lake City, UT. SME nonmeeting paper 94–654. Manuscript Aug., 1994. Discussion of this peer-reviewed and approved paper is invited and must be submitted, in duplicate, prior to May 31, 1995.

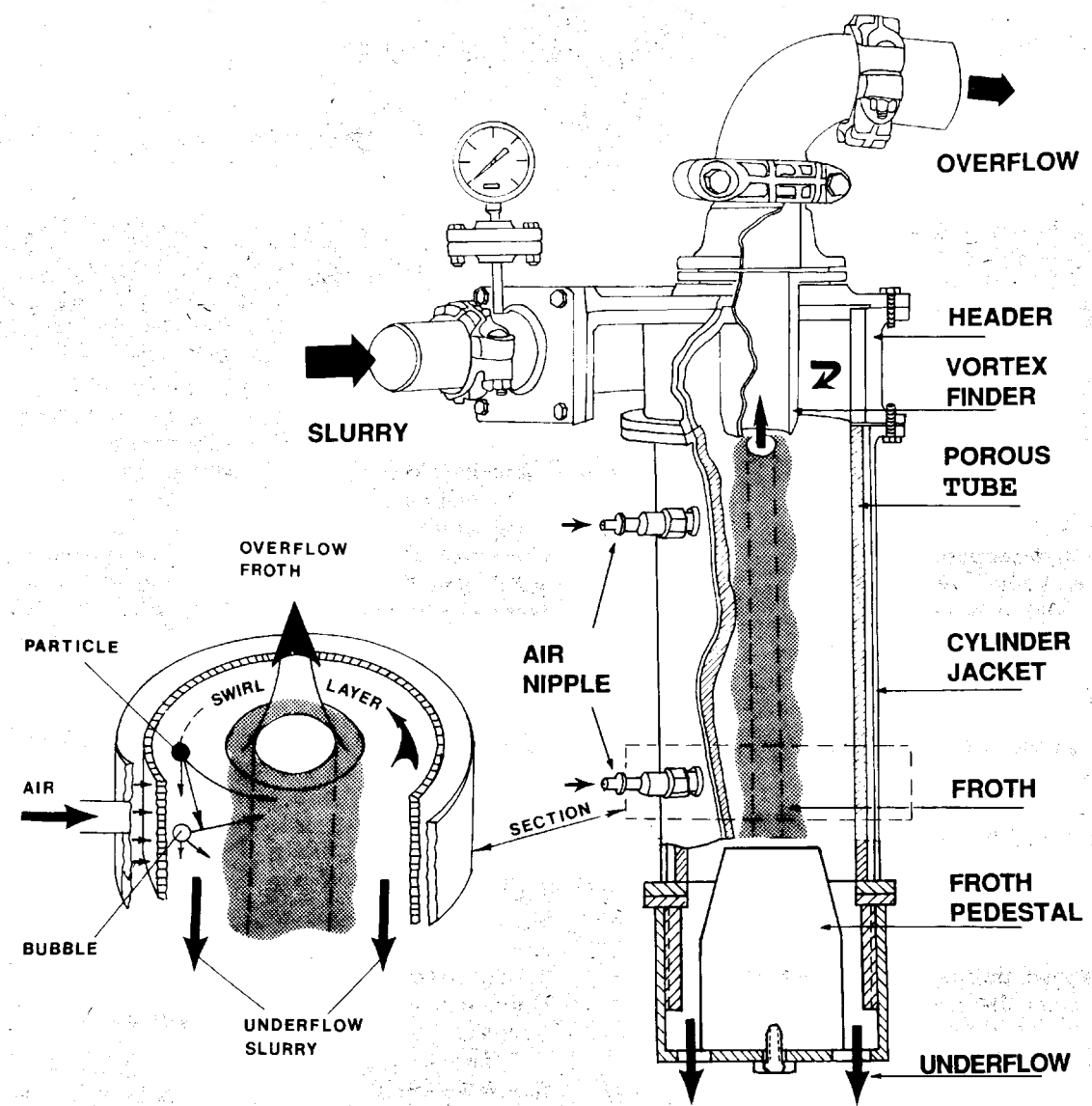

Fig. 1 — Perspective of the air-sparged hydrocyclone (ASH). (Miller et al., 1988)

bubble phase. The capacity of the ASH is thus limited by the residence time of the bubble phase. However, no efforts were made to study flow characteristics in the ASH during actual flotation (Miller, et al., 1984b).

In another study (Hupka, et al., 1994), bubble size distribution in the ASH was studied using high-speed photography for the two-phase air-water system. It was found that an increase in frother (MIBC) concentration significantly decreased the average bubble size and narrowed the size distribution for water flow rates from 30 to 75 L/min. The surfactant minimized the effect of coalescence at the point of bubble formation. The average bubble size decreased from 400 to 200 μm when the water flow rate increased from 30 to 75 L/min at a frother concentration of 10 ppm. Larger bubbles tended to be produced at higher air flow rates. However, this effect was not very substantial.

Notwithstanding these previous studies, a thorough understanding of ASH flow behavior and its relationship to flotation performance remains incomplete. In this regard, initial efforts to characterize the ASH flow behavior using X-ray computed tomography (X-ray CT) were found to be very encouraging (Lin, et al., 1992 and Miller, et al., 1990). Therefore, further study was undertaken in 1993 to provide a more detailed understanding of ASH flow behavior and flotation performance by direct experimental observation using X-ray CT (Das and Miller, 1994). Fairly accurate quantification, in terms of density profiles along the axis and along the radius of the ASH, was found to be possible by X-ray computed tomography (X-ray CT). In addition, different flow regions, e.g., air core, froth phase and swirl layer, were identified, and their spatial extent was established (Das and Miller, 1994).

As a compliment to this X-ray CT study (Das and Miller, 1994), a detailed parametric study of ASH flotation perfor-

mance was carried out using monosized quartz particles with amine as collector, and the results are reported in this contribution. Also, the swirl flow behavior in a right-vertical plexiglass cylinder was observed, and steady-state flow characteristics for different experimental conditions were recorded by photography. The steady-state flow regimes in the ASH and in the plexiglass tube, as revealed by X-ray CT and photography, respectively, are used to explain the ASH flotation of quartz and the dependence of the flotation response to the following operating variables:

- dimensionless area ratio (A*) is the ratio of overflow opening area to underflow opening area,
- dimensionless flow-rate ratio (Q*) is the ratio of air flow rate to slurry flow rate,
- percent solids in the feed suspension,
- slurry inlet pressure,
- particle size,
- collector level, and
- suspension pH.

Experimental setup and data acquisition

An ASH-2C system, designed and manufactured by Advanced Processing Technologies Inc. of Salt Lake City, UT, was used in this study. The system consists of a KREBS inlet header with a rectangular (0.80 x 0.33-in.) inlet opening and a 0.875-in. ID vortex finder, a 1.9-in. ID porous tube (12 in. long) and an underflow tapered froth pedestal. A schematic drawing of the ASH is presented in Fig. 1. Details of the X-ray CT experimental setup are described elsewhere (Das and Miller, 1994). Quartz suspensions (100 x 200 mesh and 200 x 325 mesh) were used as feed for the ASH experiments. The slurry was prepared in a 800 L sump with the desired percent solids and the desired levels of reagent addition (e.g., frother and collector). Two LIGHTNIN mixers (ND-2, CS, 1/2 HP, 1725 RPM), manufactured by Mixing Equipment Co., Inc., kept the solids in a suspended state and homogenized the slurry such that the system was well mixed. The feed slurry in the sump was conditioned for 10 min before the ASH flotation experiments were initiated. The slurry flow rate was controlled by regulating the ASH inlet pressure with a two-way Apollo ball valve manufactured by Conbraco Industries Inc. The inlet pressure was monitored by a pressure gauge that was calibrated by measuring the volume flow rate at different pressure levels. A compressor was used to supply air to the ASH. The air was sparged through the inner porous tube, which had an average pore diameter of about 50 μm (pore size range 40 to 60 μm). The air flow rate was monitored and controlled with a rotameter (Model 10A1755A) manufactured by Fisher & Porter Company. The reagents used for this study were MIBC (supplied by Aldrich Chemicals, 99% purity) as frother and dodecyl amine (supplied by Surfactant Division, Rhone Poulenc Inc.) as collector. The frother concentration was maintained at 40 ppm (water basis) for all experiments. Unless otherwise noted, the collector concentration was kept at 800 g/t of dry solids and the particle size was 100 x 200 mesh. This same ASH system was used both for the X-ray CT measurements (Das and Miller, 1994) and for the flotation experiments described in this paper. In the case of the flotation tests, the two product streams, overflow and underflow, were sampled for different experimental conditions, filtered, dried and weighed to give the amount of solids in each stream. From this data, the recovery values were then calculated. The results are reported in the following section.

To compliment our understanding of the effect of operating variables on ASH flotation of quartz, photographs of the flow characteristics were taken in a plexiglass tube. In these experiments, the porous tube section of the ASH was replaced with a nonporous, transparent 2.4-in. ID plexiglass tube connected to the header. Using this system, the changes in flow pattern with changes in feed inlet pressure and A* were observed and recorded by photography. In these experiments, the feed consisted of water only. No air was sparged.

Results and discussion

The internal flow behavior in the ASH is characterized by three distinct flow regimes, namely, the central air core, the froth phase and the swirl layer. It was observed that for inlet pressures exceeding 7 psi, there is always an air core at the center. X-ray CT measurements revealed these features clearly. Information regarding the dimensions of the above mentioned flow regimes and the radial density profiles in the ASH, as obtained from X-ray CT measurements and subsequent image analysis, have been reported in greater detail elsewhere (Das and Miller, 1994). By studying the radial density profiles at various axial locations, the flow regimes along the entire length of the ASH can be constructed. Such representations are shown and discussed with regard to the flotation response in the following subsections.

Percent solids. The flow regimes, as revealed by X-ray CT density profiles, for 5% and 15% solids in the feed are compared in Fig. 2. It can be seen from this figure that as the solids in the feed slurry is increased from 5% to 15%, the air core shrinks, and the swirl layer thickness at the top of the ASH is reduced. For 5% solids in the feed, the froth phase is relatively narrow and does not extend down to the bottom of the ASH. In this case, the flow region in the bottom half of the ASH essentially consists of an air core and a thick swirl layer of average density 1.0 g/cc, indicating the total absence of hydrophobic quartz particles in this region.

On the other hand, the froth phase is much more extensive for the 15% solids case and extends all the way down to the bottom of the ASH, gradually diminishing in thickness. In another paper (Das and Miller, 1994), it was established that the froth phase is stabilized by the presence of hydrophobic particles, as revealed by the axial views presented in Fig. 2. The disappearance of the froth phase at the very bottom and an average swirl layer density of 1.0 g/cc at this location confirms the fact that, in the case of 15% solids, hardly any solids are present at the very bottom of the ASH. Therefore, it is expected that the solids concentration gradually decreases along the ASH length (from top to bottom) and eventually becomes almost zero at the very bottom. For example, the density of the swirl layer in the feed is shown as a function of axial position in Fig. 3 for 5% solids in the feed

It was found that more than 90% of the solids are recovered to the overflow in both cases (5% and 15% solids), as shown in Table 1. Of course, the total amount of hydrophobic solids and also the extent of the froth phase is less for the 5% case than for the 15% case. Therefore, while almost all the solids have been removed in the top portion of the ASH for 5% solids, the longer length of the ASH is required for complete flotation of the solids in the 15% solids case.

Effect of porous tube length. To examine the effect of porous tube length in further detail, flotation experiments were carried out with a shorter porous tube length (6 in.

instead of 12 in.) for different levels of operating variables, and the flotation recoveries were compared. The results with the shorter ASH are compared to the results with the longer ASH in Table 2 for 5% solids in the feed. It can be seen from Table 2 that when the conditions (i.e., A*, Q* and inlet pressure) are favorable for good flotation, comparable recoveries are obtained with the 6 and 12 in. tubes. Therefore, it is evident that under these conditions, the length of the porous tube has no noticeable impact on flotation performance when the feed contains 5% solids.

Table 3 compares the recovery values for 15% solids in the feed with the two porous tube lengths (6 and 12 in.). It can be seen from Table 3 that, under favorable conditions as discussed above, the recovery drops drastically from 92% to 56% and from 80% to 59% for the two conditions shown in Table 3 when the porous tube length is reduced to 6 in. from 12 in. Evidently, a longer porous tube is required to increase the recovery of hydrophobic quartz particles in the overflow when the feed suspension contains 15% solids.

From the preceding discussion, it can be said that for a feed containing 5% solids and when the level of the operating variables are favorable for good flotation (more than 80% recovery), the recovery obtained with the shorter ASH is comparable to that with the longer ASH. However, in the case of 15% solids, reducing the length of the porous tube from 12 in. to 6 in. resulted in a large drop in recovery. Thus, it appears that a longer ASH is required for good flotation with higher percent solids in the feed slurry. However, with a lower percent solids in the feed, a shorter ASH is sufficient to produce high recovery, depending upon the operating variables.

Dimensionless area ratio (A*). The ratio of overflow opening area to the underflow opening area is defined as A*. Examination of the results from other X-ray CT experiments reveals that the air core diameter increases substantially with a decrease in A* for 5% solids in the feed (feed density = 1.032 g/cc), as can be seen from Fig. 4. Also, a relatively thick and stable froth phase can be observed, even at the bottom of the ASH, for A* = 0.74. This observation, along with the observation that the average swirl layer density at the bottom is about 1.02 g/cc, confirms the presence of hydrophobic solids at this location.

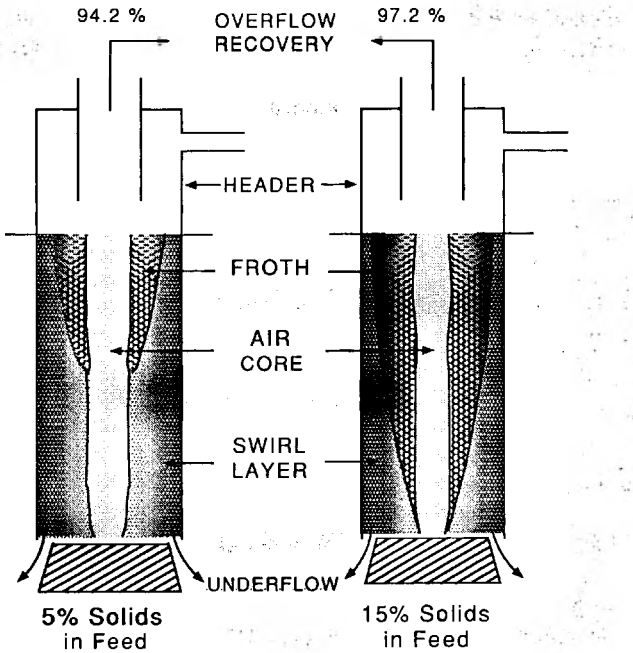

Fig. 2 — Froth features and flow regimes as revealed by x-ray CT measurements for two different solids concentrations in the feed. A* = 1.00, Q* = 4.55, inlet pressure = 10.5 psi, particle size = 100x200 mesh, and amine addition = 800 g/t.

For A* = 1.00, the froth phase is absent in the bottom half of the ASH, and an average swirl layer density of 1.0 g/cc indicates that flotation is complete. There are no solids present in this region. In fact, more than 90% recovery for A* = 1.00 and less than 70% for A* = 0.74 were obtained, as can be seen from Table 4. Generally, the swirl layer thickness can be observed to increase substantially from top to bottom for A* = 1.00, whereas the thickness of the swirl layer for A* = 0.74 does not change significantly with respect to axial position.

Flotation experiments were carried out to establish the dependence of flotation response on A* with two different solids concentrations. The results are presented in Fig. 5. Examination of Fig. 5 reveals that the recovery of hydrophobic quartz particles is a strong function of A*, especially when solids concentration in the feed slurry is high. The recovery increases relatively slowly with increases in A* for 5% solids, whereas a very steep rise can be observed for 15% solids. It is expected that at any particular elevation in the ASH, the axial velocity changes its

Table 1 — Flotation response of 100 x 200 mesh quartz particles for specified experimental conditions. Collector level: 800 g/t. Porous tube length: 12 inches.

Solids, wt%	A*	Q*	Inlet pressure, psi	Slurry flow rate, lpm	Recovery, %
5	1.00	4.55	10.5	63.2	94.2
15	1.00	4.55	10.5	63.2	97.2

Table 2 — Flotation response of 100 x 200 mesh quartz particles for specified experimental conditions with two different porous tube lengths. 5% solids in feed. collector level: 800 g/t

A*	Q*	Inlet pressure, psi	Slurry flow rate, lpm	Recovery with 12" length ASH, %	Recovery with 6" length ASH, %
1.00	4.55	10.5	63.2	91.2	88.4
1.00	6.83	6.5	46.8	80.1	80.8

Table 3 — Flotation response of 100 x 200 mesh quartz particles for specified experimental conditions with two different porous tube lengths. 15% solids in feed, collector level: 800 g/t

A*	Q*	Inlet pressure, psi	Slurry flow rate, lpm	Recovery with 12" length ASH, %	Recovery with 6" length ASH, %
1.00	4.55	10.5	63.2	92.4	56.0
1.00	6.83	6.5	46.8	80.6	59.0

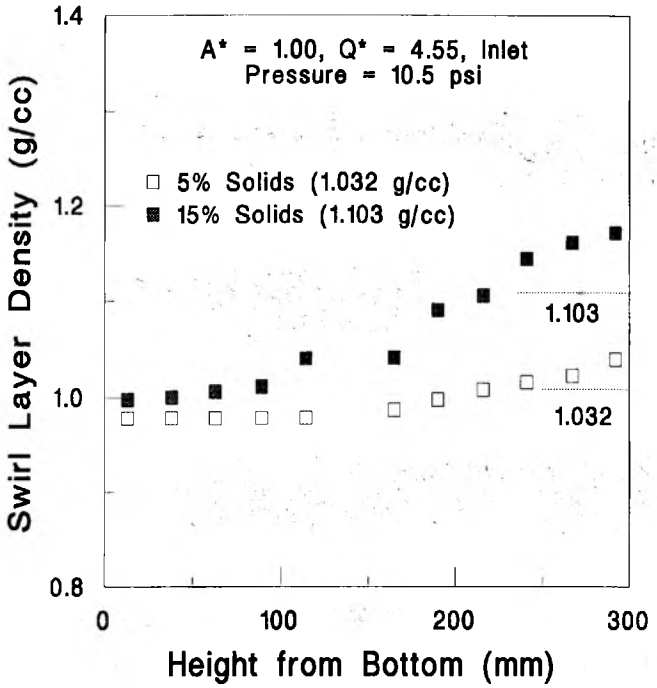

Fig. 3 — Swirl layer density as a function of axial position for two different solids concentrations in feed.

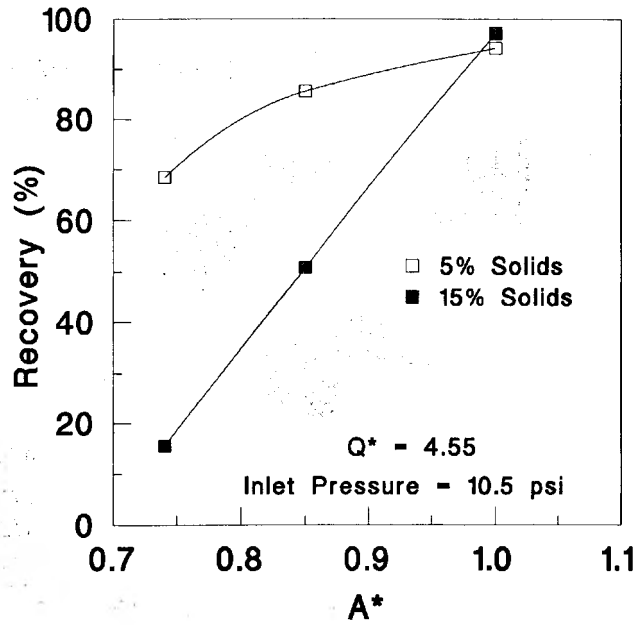

Fig. 5 — Recovery of quartz particles (100x200 mesh) as a function of A* at a collector level of 800 g/t.

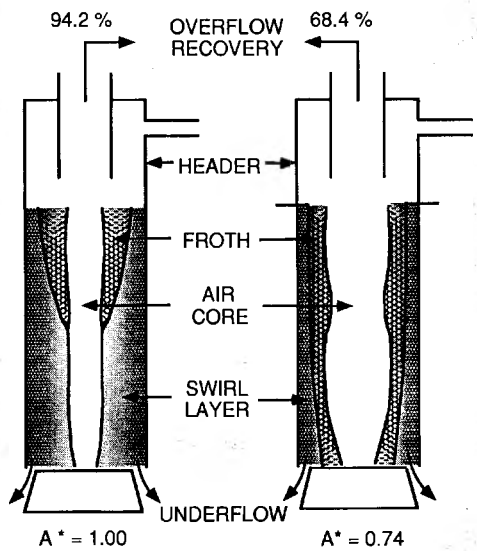

Fig. 4 — Froth features and flow regimes as revealed by x-ray CT measurements for two different A* values with 5% solids (100x200 mesh quartz particles with 800 g/t amine), Q* = 4.55 and inlet pressure =10.5 psi.

Table 4 — Flotation response of 100 x 200 mesh quartz particles for specified experimental conditions. Collector level: 800 g/ton. Porous tube length: 12 in.

Solids, wt%	A*	Q*	Inlet pressure, psi	Slurry flow rate, lpm	Recovery, %
5	1.00	4.55	10.5	63.2	94.2
5	0.74	4.55	10.5	63.2	68.4

direction at a certain radial position, depending on the experimental conditions. Therefore, a surface of zero axial velocity exists inside the ASH, and the axial flow reversal characteristics change as A* changes. It should be noted that in this study, the overflow opening area (vortex finder diameter) was not altered. Thus, a change in A* was brought about by changing the underflow opening area, and the surface of zero axial velocity may shift with regard to its radial position as the boundary conditions at the underflow exit changes. As a consequence, the amount of froth carried to the overflow will change and flotation recovery will increase or decrease accordingly. In this regard, work is in progress to locate the surface of zero axial velocity for different experimental conditions using a tracer analysis technique, and these results will be presented in a separate publication (Das and Miller, 1995).

Dimensionless flow-rate ratio (Q*). Q* is defined as the dimensionless ratio of air flow rate to slurry flow rate. The effect of Q* on the flow regimes is shown in Fig. 6 for 15% solids in the feed (feed density = 1.103 g/cc). The experimental conditions are given in the figure caption. With a low air flow rate (Q* = 2.28), as can be seen from Table 5, only 52% of the hydrophobic solids were recovered in the overflow. In this case, a very small froth region could be observed at the top of the ASH. The absence of a stable froth elsewhere and the high density (1.05 to 1.08 g/cc) of the swirl layer indicate the presence of a large amount of solids at all axial locations, which would be expected in view of the poor flotation recovery in this case. At a fixed inlet pressure, a lower value of Q* implies a lower air flow rate. Clearly, in this case there is insufficient air and the froth phase instability results in a lower recovery. At a higher air flow rate (Q* = 6.83), the froth phase stabilizes and extends all the way down to the bottom of the ASH, again gradually diminishing in thickness. It was found that, in this case, the froth phase disappears at the

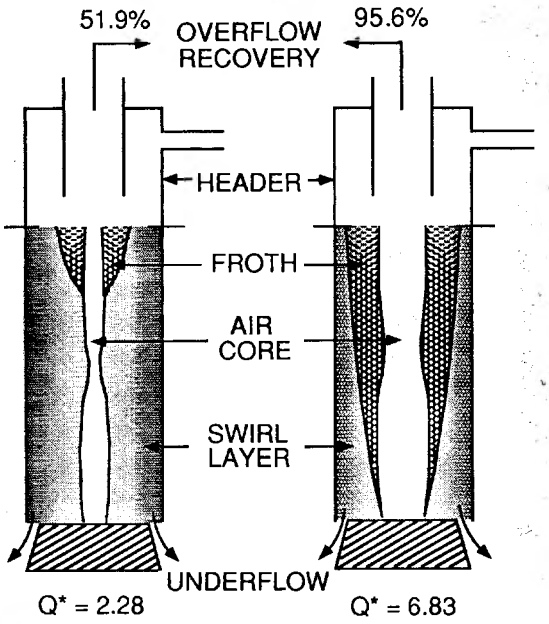

Fig. 6 — Froth features and flow regimes as revealed by x-ray CT measurements for two different Q* values with 15% solids (100x200 mesh quartz particles with 800 g/t amine), A* = 1.00 and inlet pressure = 10.5 psi.

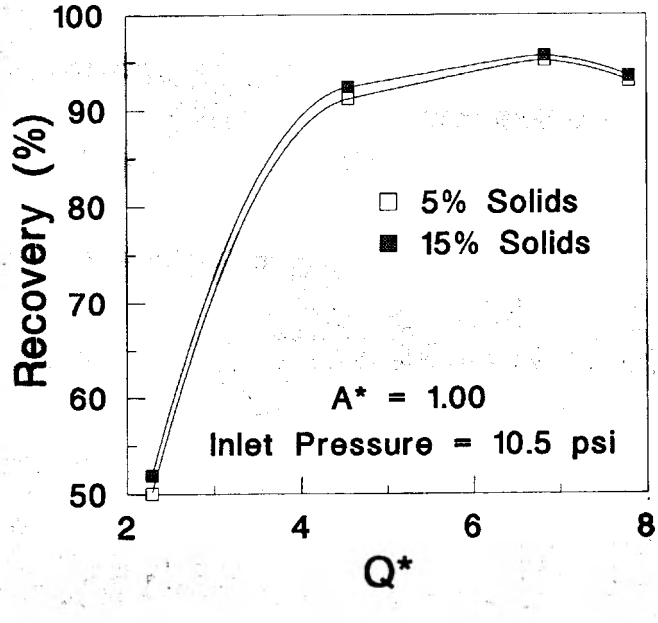

Fig. 7 — Recovery of hydrophobic quartz particles (100x200 mesh) as a function of Q* at a collector level of 800 g/t. Note that this plot was constructed from the data presented in Tables 2 and 3 for Q* = 4.55. The slope of the curve changes slightly if data from Table 1 and Fig. 2 are used.

very bottom and that the swirl layer is less dense at the bottom (about 1.0 g/cc), indicating the absence of any hydrophobic quartz particles at this location. Indeed, about 96% recovery was observed for this case, as can be seen from Table 5. Expansion of the air core with an increase in Q* is another observation that can be made from the X-ray CT data and is evident from Fig. 6.

The variation in flotation response with Q* is shown in Fig. 7. Recovery of hydrophobic quartz particles is plotted against Q* for two different solids concentrations in the feed with A* = 1.00 and an inlet pressure of 10.5 psi. It can be seen from this figure that as Q* is increased, recovery rises fast initially and then almost levels off. However, at very high Q*, the recovery drops slightly. As discussed earlier, at low Q* (low air flow rate), the air is insufficient to stabilize the froth, which results in poor recovery. As air increases (increase in Q*), the froth stabilizes, and consequently the recovery improves. It should be noted that the bubble size also increases with Q*, although not significantly (Hupka, et al., 1994). An increase in bubble size may be expected to reduce the recovery. In fact, a small decrease in recovery can be noticed at high Q* value from Fig. 7. Since the increase in bubble size is not great, its effect on recovery is not very significant.

It can also be seen from Fig. 7 that under these conditions (A* = 1.00, 10.5 psi inlet pressure), the solids concentration of the feed slurry has no noticeable impact on the flotation response. For A* = 1.00, almost the same recoveries were obtained for both 5% and 15% solids at all Q* values considered.

Inlet pressure. Of course, the pressure at which the slurry is being fed to the ASH is expected to change the flow characteristics of the ASH as it changes the inlet velocity of the slurry and hence the centrifugal force field. In this regard, the effect of inlet pressure for 15% solids in the feed was studied and is presented in Fig. 8. X-ray CT measurements revealed that a thick, stable froth phase is present all along the axis of the ASH for a lower inlet pressure (6.5 psi). The average swirl-layer density was found to be in the range 1.02 to 1.08 g/cc at most axial positions in the ASH. This confirms the presence of hydrophobic solids in the swirl layer at these locations. From Table 6, it can be seen that about 70% of the solids are recovered in the overflow for this case of 6.5 psi. Visual observations regarding the swirl-flow characteristics in a glass tube having the same inlet configuration revealed that vortex formation at 6.5 psi is barely complete. The upward axial velocities are not great in view of the low inlet velocity. The shear force and thus the bubble generation/particle collision may be reduced. Consequently, froth transport to the overflow is diminished.

Table 5 — Flotation response of 100 x 200 mesh quartz particles for specified experimental conditions. Collector level: 800 g/t. Porous tube length: 12 in.

Solids, wt%	A*	Q*	Inlet pressure, psi	Slurry flow rate, lpm	Recovery, %
15	1.00	2.28	10.5	63.2	51.9
15	1.00	6.83	10.5	63.2	95.6

Table 6 — Flotation response of 100 x 200 mesh quartz particles for specified experimental conditions. Collector level: 800 g/t Porous tube length: 12 in.

Solids, wt%	A*	Q*	Inlet pressure, psi	Slurry flow rate, lpm	Recovery, %
15	1.00	4.55	10.5	63.2	97.2
15	1.00	4.55	6.5	46.8	69.9

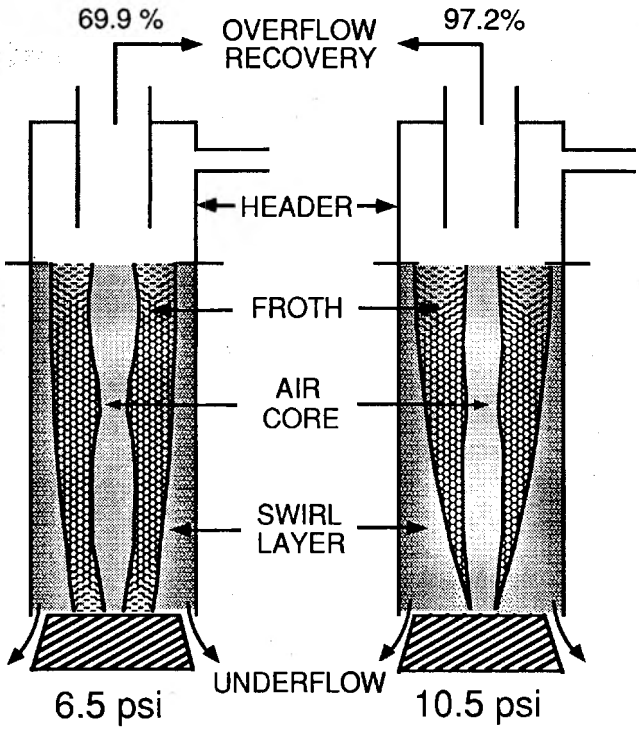

Fig. 8 — Froth features and flow regimes as revealed by x-ray CT measurements for two different inlet pressures with 15% solids (100x200 mesh quartz particles with 800 g/t amine), A* = 1.00 and Q* = 4.55.

On the other hand, the higher shear rate at 10.5 psi facilitates a higher particle/bubble collision frequency. The velocities are greater in magnitude, which facilitates transport of the froth phase to the overflow giving higher recovery. The froth phase, in this case, gradually decreases in thickness down the axis of the ASH and eventually disappears at the bottom most part of the ASH, as can be seen from Fig. 8. The average swirl-layer density at the bottom is about 1.0 g/cc, indicating the absence of solids at this location. In this case, about 97% recovery was obtained. It was found that the air core shrinks as the slurry pressure increases. This feature has also been observed visually in the case of swirl flow through a plexiglass tube, which will be discussed later.

From the above figures and discussion, it appears that there is a relationship between the thickness of the froth phase and the solids concentration when a stable froth is formed. In general, the froth phase thickness for 15% solids was found to be greater than the froth phase thickness for 5% solids when the conditions are suitable to stabilize the froth phase.

Regarding flotation recovery, the influence of inlet pressure Q* and solids concentration in the feed have been summarized graphically in Fig. 9. Three very interesting aspects of ASH flotation can be observed from this figure. First, a comparison between the results in (a) for 5% solids and in (b) for 15% solids reveals that when A* is maintained at a high level (A* = 1.00), the solids concentration in the feed (within the range considered) has no noticeable impact on the flotation response. Second, at any Q* value, the recovery passes through a maximum as inlet pressure is increased from 6.5 to 16.5 psi. The recovery increases first and then starts to drop beyond 10 psi. Third, with respect to Q*, there appears to be an optimum level for this dimensionless variable. At any inlet pressure, the recovery increases with Q* up to a certain point (Q* = 6.83), and beyond this point it starts to decrease slightly.

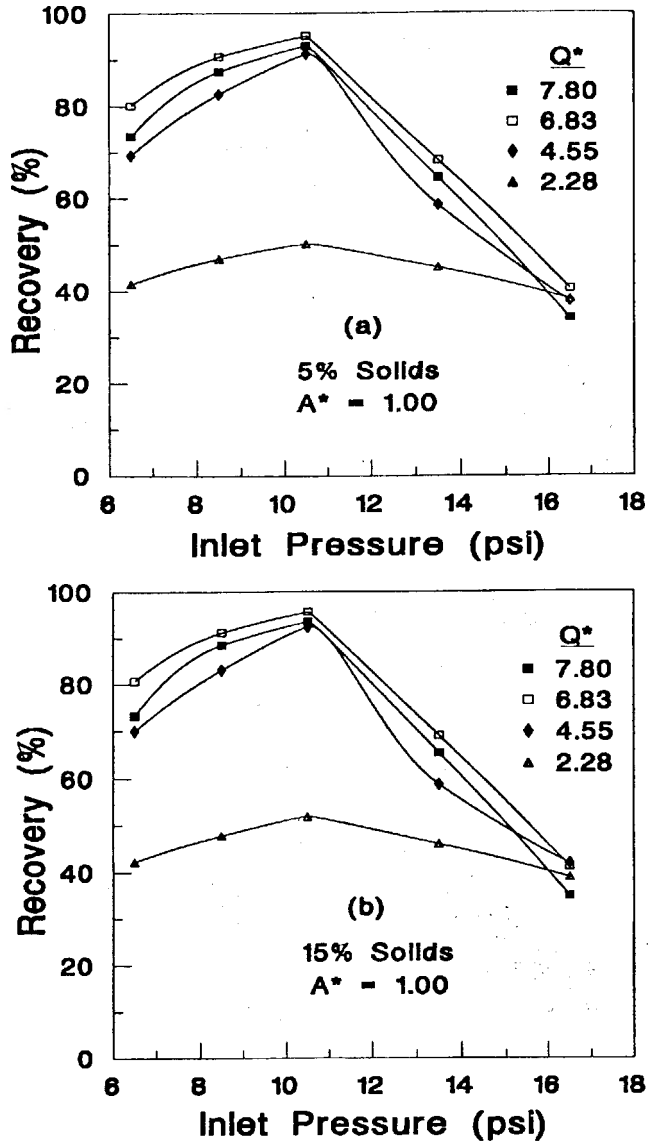

Fig. 9 — Recovery of quartz particles (100x200 mesh) as a function of inlet pressure for various Q* values and two different solids concentrations in feed at a collector level of 800 g/t. Note that this plot was constructed from the data presented in Tables 2 and 3 for Q* = 4.55. The slope of the curve changes slightly if data from Table 1 and Fig. 2 are used.

These observations lead to the following phenomenological explanations. First, at a given Q*, an increase in inlet pressure enhances the shear rate for improved bubble generation, and the higher velocities facilitate froth transport to the overflow. In view of the high centrifugal force in the ASH, bubble generation is expected to be governed by the shear at the wall. At higher inlet pressures, smaller bubbles are expected to be ripped off from the wall. The smaller size of the bubbles enhances flotation and consequently the recovery improves. However, beyond a certain inlet pressure, the resulting tangential velocity, and hence the centrifugal force, for detachment may be too high for the bubble/particle aggregate to remain stabilized. Also, no further decrease in bubble size is possible. Under such conditions, detachment occurs, resulting in a drop in recovery. Second, at a given inlet pressure, as Q* is increased, the concentration of bubbles increases because of the increased air flow rate. This results in enhanced recovery. However, as found in earlier research

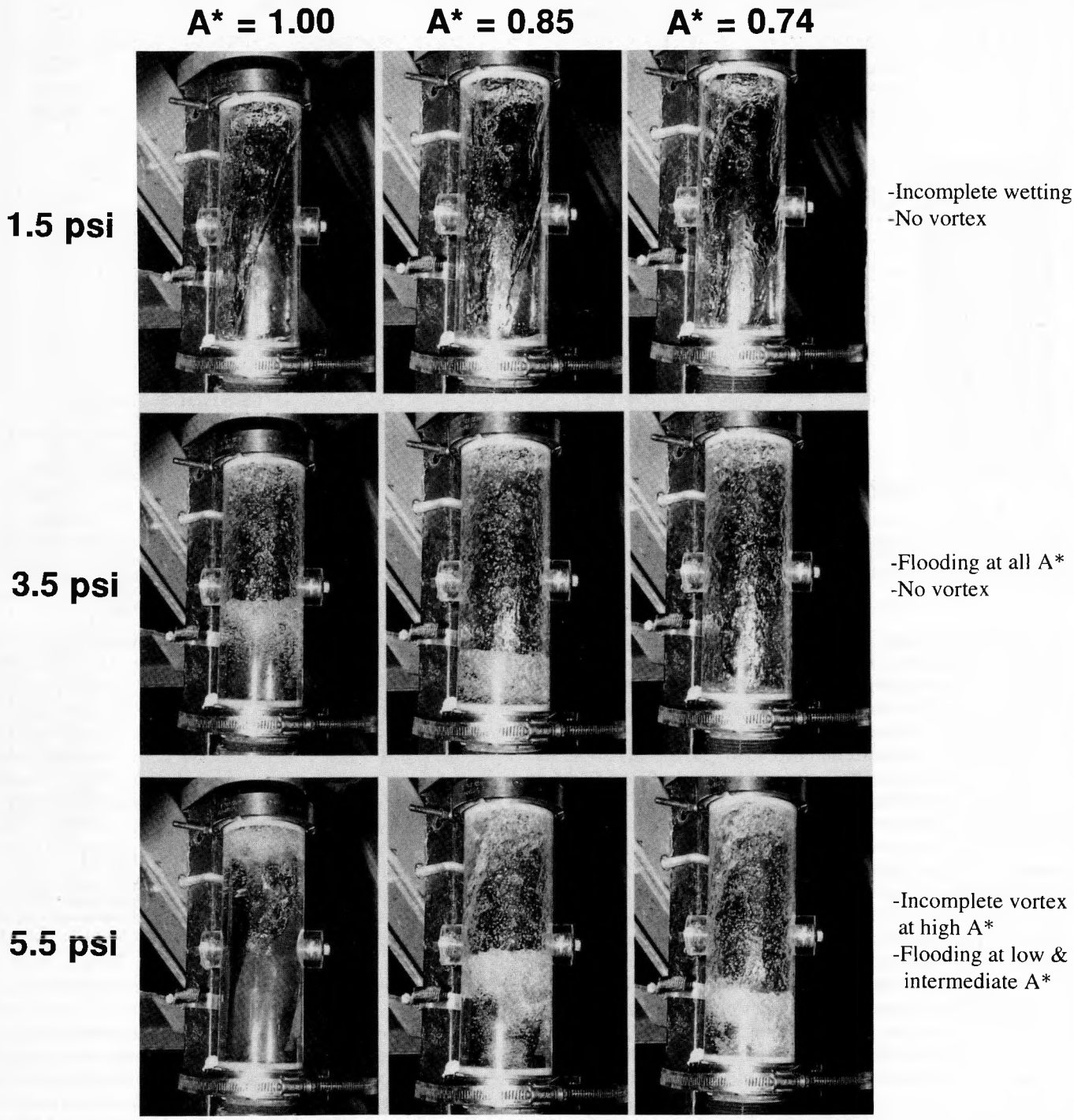

Fig. 10(a) — Variation in swirl flow behavior with A* at low inlet pressures for water flow in a right vertical plexiglass tube.

(Hupka, et al., 1994), the bubble size increases with an increase in air flow rate. Thus, at higher air flow rates (higher Q*), the bubble concentration may reach a constant value with the increase in air simply being accommodated by the generation of bubbles of larger size. This is detrimental to flotation. However, since the bubble size does not increase substantially with Q*, the drop in recovery is also small. From Fig. 9, it may be seen that there is a trade off involved both with respect to inlet pressure and Q*. It appears that, for the flotation of 100 x 200 mesh quartz particles, the system reaches an optimum at an inlet pressure of about 10 psi and a Q* value of about 7.00.

Flow in a transparent right-vertical tube. Visual observations of the flow patterns in a plexiglass tube are represented by the photographs shown in Figs. 10(a) and 10(b). The three columns are for A* = 1.00, 0.85 and 0.74, respectively. The rows are for (a) inlet pressures 1.5, 3.5, and 5.5 psi and (b) inlet pressures 7.5, 10.5 and 13.5 psi, respectively. It can be seen from Fig. 10(a) that, for all A* values, wetting

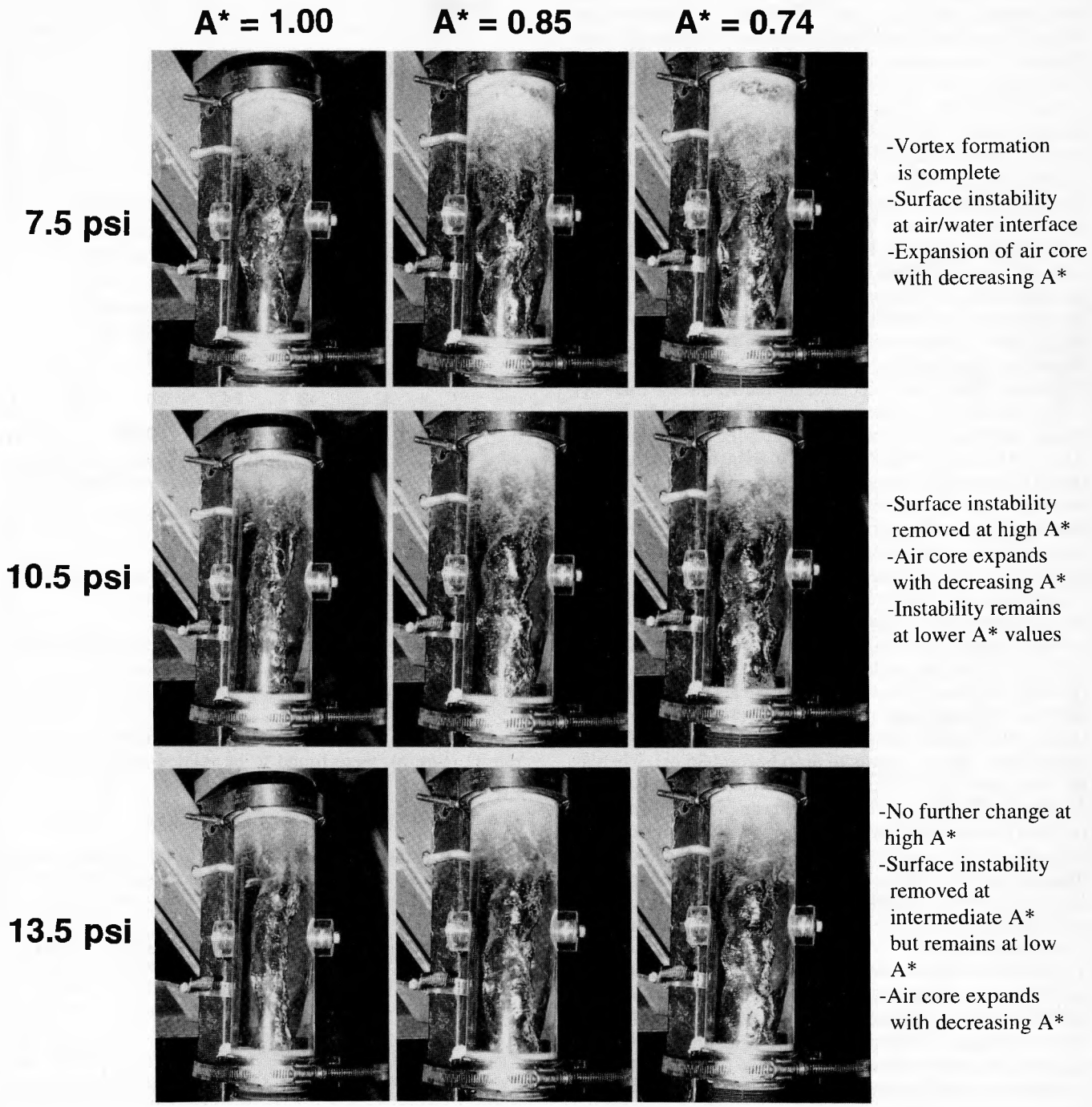

Fig. 10(b) — Variation in swirl flow behavior with A* at high inlet pressures for water flow in a right vertical plexiglass tube.

of the tube surface is incomplete at 1.5 psi. There is no vortex formation at 3.5 psi, and the tube is flooded at the bottom at all A* values.

For A* = 0.74, the vortex formation is complete at 7.5 psi (see Fig. 10(b)). The effect of pressure-drop oscillation (Yadigaroglu and Chan, 1979) is reflected in the air core surface. For such a low value of A* (A* = 0.74), the underflow opening area is large and hence the water split to the overflow is small. In this case, the fluctuating volume flow rate in the overflow stream is indicative of a fluctuating axial pressure drop. Because of this unsteady nature of the pressure drop, surface instabilities result. A wave pattern, three-dimensional in character, forms at the air core/froth interface. This wave pattern can be seen from Fig. 10(b) at all inlet pressures for A* = 0.74.

For A* = 0.85, although the vortex formation is complete at 7.5 psi, the effect of pressure-drop oscillation can be observed at the air-water interface from Fig. 10(b). The wave

pattern forms at the interface owing to fluctuating pressure drop characteristics. However, at very high inlet pressure (13.5 psi), the pressure drop and the volume flow rate to the overflow stream stabilize to a great extent. Therefore, at this inlet pressure, with A* = 0.85, the surface instabilities are reduced substantially resulting in a near-cylindrical air core. It can also be seen from this figure that the air core shrinks with inlet pressure.

For A* = 1.00, vortex formation is incomplete at 5.5 psi (see Fig. 10(a)). At 7.5 psi vortex formation is complete and an air core extending to the bottom of the tube is clearly visible from Fig. 10(b). At this high value of A* (A* = 1.00), the underflow opening is relatively small and the flow rate to the overflow stream was found to be steady and even at lower values of inlet pressure. The wave pattern, not so prominent, at the air-water interface can be seen only at 7.5 psi. Above this inlet pressure, the pressure drop stabilizes completely and the surface instabilities disappear, resulting in a cylindrical air core. The air core shrinks a little with inlet pressure. However, no further change is noticeable above 10.5 psi.

Comparisons at any inlet pressure between these three A* values reveals that the air core expands as A* is decreased. Vortex formation is complete at about 7 psi for all cases. At lower A* values (A* = 0.85 and 0.74), a wave pattern forms at the air-water interface, even at high inlet pressures, and the flow instabilities are very prominent. At a high A* value (A* = 1.00), the flow is more stable and the wave pattern disappears from the interface at lower inlet pressures. The pressure-drop oscillations are no longer visible at the high A* value.

Particle size. Figure 11 shows the effect of particle size on ASH flotation of quartz. Fairly high recovery can be achieved even at a low Q* (recovery is about 70% at Q* = 2.28) in the case of smaller particles (200 x 325 mesh). The recovery of 200 x 325 mesh quartz particles is fairly insensitive to inlet pressure over a wide range (10 to 35 psi) at any Q*, as can be seen from Fig. 11. Also, for these smaller particles the recovery starts to drop beyond 36 psi, whereas for larger particles (100 x 200 mesh) the recovery starts to drop beyond 10 psi. This observation can be explained by the fact that the centrifugal acceleration required for detachment is greater in the case of smaller particles, because of their lower mass. Therefore, the stability of the bubble/particle aggregates is maintained even at high inlet pressures (~36 psi), and the hydrophobic quartz particles are transported into the froth phase.

On the other hand, for the larger particles the centrifugal acceleration required for detachment is smaller, and the bubble/particle aggregates become unstable at a relatively low inlet pressure (~10 psi). Bubble detachment begins to take place at an inlet pressure exceeding 10 psi, resulting in a drop in recovery. In an earlier publication (Miller, 1991), it was established from theoretical considerations that the maximum diameter of a particle that can be floated in a centrifugal field should be inversely proportional to the square root of centrifugal acceleration. From a balance of the surface tension and the centrifugal force acting on the particle/bubble aggregate, the following relationship was found, and the maximum size particle to be floated should vary inversely with the tangential velocity:

$$d_{max} = C[V^2/R]^{-1/2} \quad (1)$$

where,

d_{max} = maximum particle size to be floated
V = tangential velocity

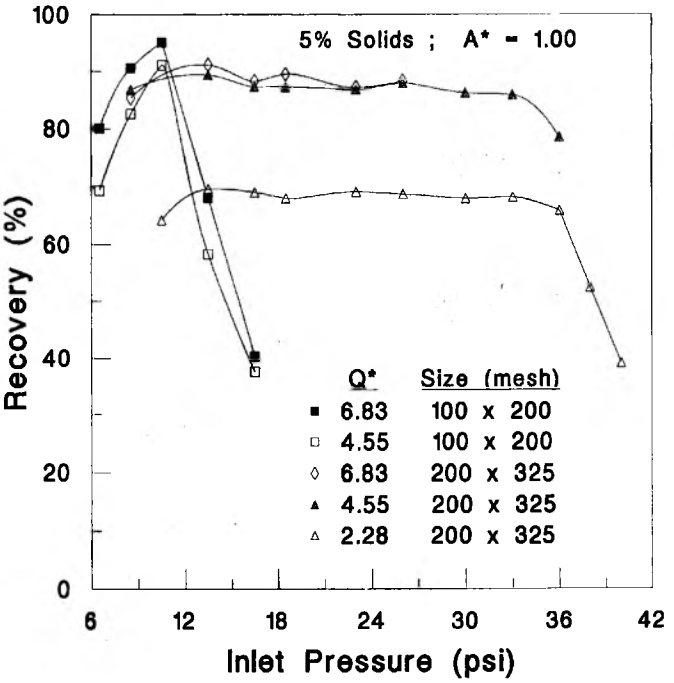

Fig. 11 — Variation in the recovery of hydrophobic quartz particles with inlet pressure for various Q* values and two different particle sizes at a collector level of 800 g/t.

R = radius of the ASH
C = constant which includes surface tension, particle density, bubble size, contact angle, etc.

Thus, the ratio of maximum size particles to be floated at two different inlet pressures should be as follows:

$$d_{1,max}/d_{2,max} = V_2/V_1 \quad (2)$$

In this study, the inlet pressure P (psi), and the slurry flow rate Q (L/min), were found to be related in the following manner:

$$Q = 23.66P^{1/2} - 13.47 \quad (3)$$

The flow rate Q (L/min) is related to the inlet area, A_{inlet} (cm^2), and the inlet velocity, V_{inlet} (cm/sec), as follows:

$$Q = (A_{inlet}\, V_{inlet})\, (60/1000) \quad (4)$$

And, for these experiments, the inlet area was constant.

$$A_{inlet} = 1.716\ cm^2 \quad (5)$$

Therefore, from Eq. (3):

$$V_{inlet} = 229.8P^{1/2} - 130.8 \quad (6)$$

where the inlet velocity is in cm/sec and the inlet pressure is in psi.

It is expected that the ratio of the d_{max} values should be equal to the inverse ratio of the tangential velocities, as determined by the corresponding pressures. That is, approximating the velocities by the inlet velocity in (2),

$$\frac{d_{max,\,p=p1}}{d_{max,\,p=p2}} = \frac{V_{inlet,\,p=p2}}{V_{inlet,\,p=p1}} = \frac{(229.8P_2^{1/2} - 130.8)}{(229.8P_1^{1/2} - 130.8)} \quad (7)$$

Equation (7) describes the relationship between the feed inlet pressure and the maximum particle size that can be floated in the resulting centrifugal field. Thus, from the data presented in Fig. 11, $d_{max,\,10\,psi} = 105\ \mu m$ and $d_{max,\,36\,psi} = 47.5$

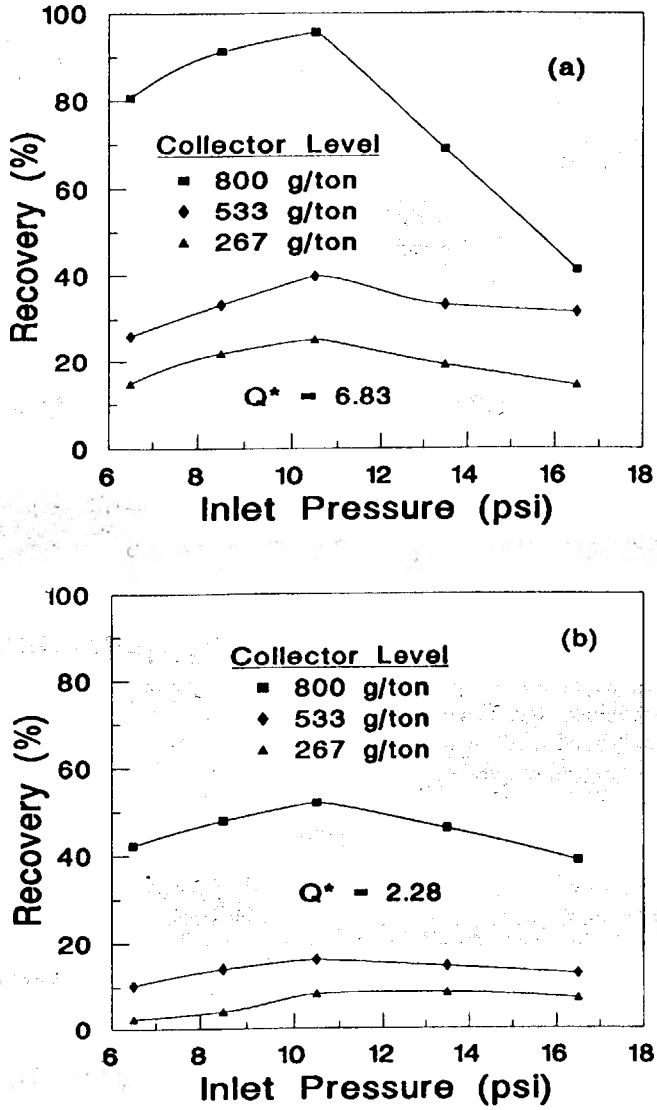

Fig. 12 — Variation in the recovery of hydrophobic quartz particles (100x200 mesh) with inlet pressure for various collector levels at a pH of 7.4, an A* of 1.00 and (a) Q* = 6.83 (b) Q* = 2.28.

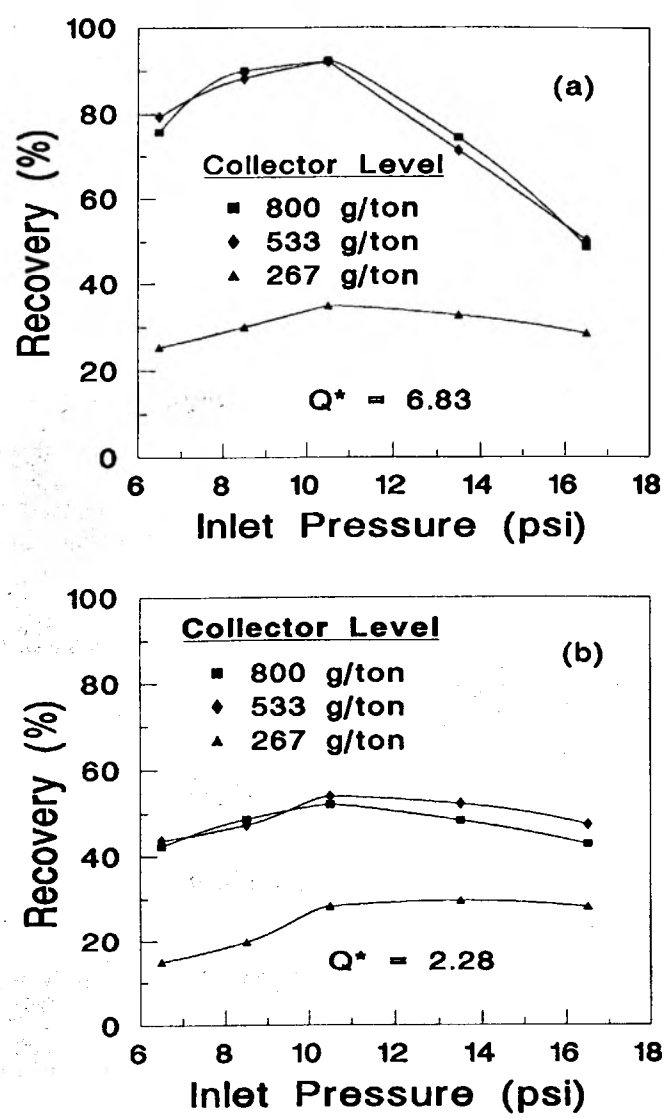

Fig. 13 — Variation in the recovery of hydrophobic quartz particles (100x200 mesh) with inlet pressure for various collector levels at a pH of 10.1, an A* of 1.00 and (a) Q* = 6.83 (b) Q* = 2.28.

μm, the validity of Eq. (7) can evaluated and substantiated by the experimental results. For example, using the d_{max} values and a pressure of 10 psi, the other pressure can be calculated to be 39.7 psi, which agrees rather well with the experimental value of 36 psi.

The observations from Fig. 11, that the recovery drops at about 10 psi for the larger (100 x 200 mesh) particle size and at about 36 psi for the smaller (200 x 325 mesh) particle size, corroborate the earlier results and analysis about the maximum size of particles that can be recovered by ASH flotation (Miller, 1991). It should be noted that in the above calculations, the tangential velocity has been approximated by the maximum tangential velocity (inlet velocity).

Collector level. Flotation experiments were also carried out to establish the influence of collector concentration on flotation response. These tests were done as a function of inlet pressure at two different Q* values, three different collector concentrations, 5% solids (100x200 mesh) in the feed, and A* = 1.00. The pH of the feed suspension was maintained at a constant level of 7.4 for all these tests. A graphical representation of these results is given in Fig. 12 for (a) Q* = 6.83 and (b) Q*=2.28. It can be seen from this figure that, in general, an increase in the amount of collector increases the ASH flotation recovery. At all collector levels, the recovery rises initially with inlet pressure and, beyond a critical inlet pressure, it starts to drop. The highest recoveries are obtained in all cases at the highest level of collector concentration (800 g/t). The increase in recovery when the collector concentration is increased from 533 to 800 g/t is substantial in both cases, as can be seen from the data presented in Fig. 12.

Examination of Fig. 12 also reveals that at a low Q* value (Q* = 2.28), the air flux is insufficient, and hence even with a high collector concentration (800 g/t) only about 50% recovery was achieved.

When the air flux is increased (Q* = 6.83), the recovery also increased. However, with lower collector concentrations (267 and 533 g/t), about 20% and 40% solids were recovered in the overflow even at a high Q* (Q* = 6.83). It appears that, at this pH, quartz surface coverage by dodecyl amine is inadequate with 267 g/t. With a higher collector concentration (533 g/t), the

surface coverage becomes better. Under this condition, when the air flux becomes adequate at a high Q* (Q* = 6.83), a higher recovery results, as can be seen from Fig. 12(a). Further increases in collector concentration (to 800 g/t) at this pH increases surface coverage and a still better recovery results. Again, at a very high inlet pressure, detachment starts to occur, which causes a drop in the recovery.

Suspension pH. To study the effect of pH on flotation response, ASH experiments were carried out at a different pH value (pH = 10.1). Sodium hydroxide was added to the pulp and the pH was raised to 10.1. Flotation tests were done as a function of inlet pressure at two different Q* values, three different collector concentrations, 5% solids (100x200 mesh) in the feed, and A* = 1.00. The test results for (a) Q* = 6.83 and (b) Q* = 2.28 are presented graphically in Fig. 13 and discussed below.

It can be seen that, at a high value of Q* (Q* = 6.83), the air flow rate is adequate to stabilize the froth phase. At this Q*, when the collector concentration was increased from 267 to 533 g/t, a marked increase in recovery was observed as can be seen from Fig. 13(a). However, further increases in collector concentration (to 800 g/t) did not result in any further increase in recovery.

At a low value of Q* (Q* = 2.28), insufficient air flow limits the recovery to low values because of froth instability. However, when the collector concentration increased from 267 to 533 g/t, the recovery also increased, although not substantially (see Fig. 13(b)). Further increases in collector concentration resulted in a small drop in recovery.

Comparison of Fig. 13 (suspension pH = 10.1) with Fig. 12 (suspension pH = 7.4) reveals that the flotability of quartz increases at lower collector levels as the pulp becomes more alkaline (Fuerstenau and Raghavan 1978). Under this condition, a smaller amount of collector is sufficient to achieve good flotation. Thus, it can be concluded that a more alkaline pulp reduces the consumption of collector. However, at a high pH (pH = 10), beyond a collector level of about 700 g/ton (~ 104 M), a drop in recovery may be expected from surface chemistry considerations (Laskowski, et al., 1988). Indeed, at a collector level of 800 g/t and a pH of 10, a small drop in recovery has been observed (see Fig. 13). A detailed discussion of the surface chemistry aspects of the amine/quartz system is beyond the scope of this paper.

In this research, most of the experiments were carried out at a high collector concentration of 800 g/t of dry solids and a suspension pH of 7.4. It should be noted that the objective of this research was not to optimize the level of reagent addition but rather to examine the effect of multiphase flow phenomena on ASH flotation. It is evident from the data presented in Figs. 12 and 13 that the collector can be reduced substantially by appropriate control of suspension pH.

Summary and conclusions

Air sparged hydrocyclone flotation of monosized quartz with dodecyl amine as collector is strongly dependent on the characteristics of the multiphase fluid flow, which, in turn, depends on the levels of the operating variables. The effects are manifested in the shape of the air core and its dimension, the stability of the froth phase and the swirl layer thickness. In addition, the system is further characterized by the density of each flow regime and, of course, the recovery of hydrophobic quartz particles in the overflow.

The flotation efficiency was found to be related to the characteristic features of the flow regimes, namely, air core, froth phase and swirl layer. In general, it was observed that the presence of hydrophobic solids greatly enhances froth stability. Operating and design considerations which limit froth transport to the overflow and lead to stabilization of the froth phase at the bottom of the ASH generally result in the loss of froth and hydrophobic particles to the underflow, which results in poor flotation recovery.

Percent solids. The air core was found to expand with decreasing solids concentration in the feed. The thickness and spatial extent of the froth phase appears to be proportional to the solids concentration when a stable froth is formed. Consequently, the residence time required for good flotation, and thus the length of the porous tube, depend on the solids concentration of the feed suspension.

Dimensionless area (A*). An increase in A* causes the air core to shrink and flotation performance was found to improve with an increase in A*. Froth transport characteristics are more favorable when A* is greater, resulting in a higher recovery. A high value of A* was also found to eliminate instabilities at the air core/froth phase interface, rendering the air core almost cylindrical.

Dimensionless flowrate (Q*). A low value of Q* destabilizes the froth due to an insufficient supply of air. As Q* is increased up to some appropriate level, depending on other variables, the flotation rate appears to increase, and the stabilized froth results in the capture and recovery of more hydrophobic quartz particles.

Inlet pressure. In the case of the ASH-2C, vortex formation is complete at about 7 psi inlet pressure. The instabilities at the air core-slurry interface are reduced with increasing inlet pressure. A high inlet pressure enhances froth transport. But too high a tangential velocity results in the disengagement of the bubble-particle aggregate, due to the increased centrifugal force, and thus under such conditions poor recovery occurs.

Particle size. It was confirmed from this study that the maximum size of quartz particle that can be floated in a centrifugal field is inversely proportional to the square root of the centrifugal acceleration. Because of the higher centrifugal force required for detachment of smaller particles, the froth phase is much more stable, even at high inlet pressures. Therefore, in the case of particles of smaller size (200 x 325 mesh), transport of the mineralized bubble to the overflow stream occurs without significant detachment under severe flow conditions, and good recovery is achieved, even at an inlet pressure of 30 psi. On the other hand, particles of larger size (100 x 200 mesh) can not be floated efficiently at inlet pressures exceeding 15 psi.

Collector level. At a low pH (pH = 7.4), relatively high levels of amine collector addition were necessary to achieve complete recovery. As expected, quartz was found to float better in a more alkaline medium at a lower level of collector addition. Collector consumption can be reduced by appropriate control of the suspension pH and by the use of large diameter ASH units.

Acknowledgments

The authors wish to acknowledge the financial support from the Department of Energy, Grant No. DE-FG22-

9OPC90311, and the National Science Foundation, Grant No. CTS 9000406.

References

Das, A., and Miller, J.D., 1994, "Swirl flow characteristics and froth phase features in air-sparged hydrocyclone flotation as revealed by X-Ray CT analysis," *International Journal of Mineral Processing*. Submitted for publication.

Das, A., et al., 1993, "Fluid motion in air-sparged hydrocyclone: Single-phase measurements and calculations of tangential velocity of swirl flow in a right vertical cylinder," *Scandinavian Journal of Metallurgy*, Vol. 22, pp. 254-259.

Fuerstenau, D.W., and Raghavan, S., 1978, "The surface and crystal chemistry of silicate minerals and their flotation behavior," Freib. Forsch. - H. A. 593. Hrsg.: Rektor der Bergakademie Freiberg, Leipzig: VEB Deutscher fur Grundstoffindustrie, pp. 75-109.

Gopalakrishnan, S., Ye, Y., and Miller, J.D., 1991, "Dimensionless analysis of process variables in air-sparged hydrocyclone (ASH) flotation of fine coal," *Coal Preparation: An International Journal*, Vol. 9, pp. 169-184.

Hupka, J., et al., 1994, "Bubble size distribution in air-sparged hydrocyclone," *Proceedings of 12th International Coal Preparation Congress*, Cracow, Poland, pp. 1267.

Laskowski, J.S., Vurdela, R.M., and Liu, Q., 1988, "The colloid chemistry of weak-electrolyte collector flotation," *XVI International Mineral Processing Congress*, Forssberg, E., ed, Elsevier Science Publishers B. V., Amsterdam, pp. 703-715.

Lin, C.L., Miller, J.D., and Cortes, A.B., 1992, "Applications of X-Ray computed tomography in particulate systems," KONA, *Powder and Particle*, No. 10, pp. 88-95.

Loader, A.J., 1981, "Instability and Turbulence in Confined Swirling Flow Investigated by Laser Doppler Anemometry," Ph.D. dissertation, Southampton University, Department of Mechanical Engineering, pp. 7-16.

Miller J.D., and Kinneberg, D.J., 1984a, "Fast flotation in an air-sparged hydrocyclone," *Proceedings of MINTEK 50*, Johannesburg, South Africa, Vol. 1, pp. 373.

Miller J.D., and Ye, Y., 1989, "Froth characteristics in air-sparged hydrocyclone flotation," *Mineral Processing and Extractive Metallurgy Review*, Vol. 5, pp. 307–329.

Miller, J.D., 1991, "The status of air-sparged hydrocyclone flotation technology," *4th Asian Symposium on Mineral Processing*, Manila, Philippines.

Miller, J.D., et al., 1984b "Fluid flow phenomena in the air-sparged hydrocyclone," *XV International Mineral Processing Congress*, Cannes, France, Vol. II, p. 87.

Miller, J.D., et al., 1988, "Design and operating variables in flotation separation with the air-sparged hydrocyclone," *Proceedings of XVI International Mineral Processing Congress*, K.S.E. Forssberg, ed., Stockholm, Sweden, pp. 499-510.

Miller, J.D., Lin, C.L. and Cortes, A.B., 1990, "Review of X-ray computed tomography and its applications in mineral processing," Mine*ral Processing and Extractive Metallurgy Review*, Vol. 7, pp. 1-18.

Yadigaroglu, G. and Chan, K.C., 1979, "Analysis of flow instabilities," *Two Phase Flow Dynamics: Japan-US Seminar 1979*, A.E. Bergels and S. Ishigai, eds., Hemisphere Publishing Co., pp. 353.

Ye, Y., et al., 1988, "Development of the air-sparged hydrocyclone - A swirl flotation column," Proc*eedings of International Column Flotation Symposium*, AIME/SME, Phoenix, AZ, Chapter 34, pp. 305-313.